Manipulation of subsurface carbon nanoparticles in $Bi_2Sr_2CaCu_2O_{8+\delta}$ using a scanning tunneling microscope

A. J. Stollenwerk,* N. Hurley, B. Beck, K. Spurgeon, and T. E. Kidd
University of Northern Iowa, Department of Physics, 215 Begeman Hall, Cedar Falls, Iowa 50614-0150, USA

G. Gu
Condensed Matter Physics and Materials Science Department, Brookhaven National Laboratory, Upton, New York 11973-5000, USA

(Received 3 December 2014; revised manuscript received 13 February 2015; published 19 March 2015)

We present evidence that subsurface carbon nanoparticles in $Bi_2Sr_2CaCu_2O_{8+\delta}$ can be manipulated with nanometer precision using a scanning tunneling microscope. High-resolution images indicate that most of the carbon particles remain subsurface after transport observable as a local increase in height as the particle pushes up on the surface. Tunneling spectra in the vicinity of these protrusions exhibit semiconducting characteristics with a band gap of approximately 1.8 eV, indicating that the incorporation of carbon locally alters the electronic properties near the surface.

DOI: 10.1103/PhysRevB.91.125425 PACS number(s): 68.37.Ef, 73.21.Ac, 73.22.−f

I. INTRODUCTION

Researchers have developed a number of innovative techniques that employ the scanning tunneling microscope (STM) to manipulate surfaces on the nanometer scale. The most straightforward method is through a physical impact with the tip, previously used to study surface hardness [1,2]. Electrochemical etching with the tip has been used to carve out nanostructures on the surface of certain crystals by selectively removing material [3,4]. Perhaps most well known is the ability to move individual atoms using a tunable bond between the tip and the atom [5–12]. Control at this scale was limited to surfaces until manipulation of individual dopants was first demonstrated in Pd when an STM tip was used to vertically transport H from bulk to subsurface sites by elevating the tip voltage [13]. Recently, an additional degree of control was demonstrated when interstitial Zn was pulled toward the surface of ZnO(0001) and later pushed back into the bulk by reversing the polarity of the tip bias [14]. The ability to manipulate individual dopants is highly desirable to attain control over local electronic properties, especially in layered materials which are both easy to manipulate through doping within interlayer sites and display a rich variety of electronic phases such as high-temperature superconductivity, topological insulators, and density wave states. Local control of electronic states at the nanoscale can lead to interesting phase boundary interfaces. For example, one could in principle use local control of dopants in superconducting materials to create nanoscale insulating areas in which the superconducting ground state is inhibited. Lateral control over the dopant distribution would enable the creation of a patterned array of Josephson junctions or other components of superconducting circuitry that could be used in quantum computing applications [15,16]. One could also use the formation of nanoscale insulating regions to examine interfacial transport properties in novel electronic ground states [17,18].

In this article, we demonstrate the ability to move carbon particles between the layers of $Bi_2Sr_2CaCu_2O_{8+\delta}$ with nanometer precision. Tunneling spectra indicate that the inclusion of carbon causes the normally metallic substrate to exhibit semiconducting properties on a local scale. Subsurface nanostructures can be constructed through the ordered accumulation of these particles as the tip is rastered across the surface. These subsurface structures produce observable protrusions on the surface the height of which can be controlled by adjusting the tip bias and tunneling current in addition to the dwell time. Lateral dimensions of these structures are controlled by the size of the scan area with lower limits down to roughly 10 nm depending on the quality of the tip. Bias-dependent data suggest that the electric field generated by the tip is able to penetrate the surface of BSCCO due to the nonconductive nature of the top two layers, allowing electric forces to manipulate near surface carbon.

II. EXPERIMENTAL

Optimally doped $Bi_2Sr_2CaCu_2O_{8+\delta}$ single crystals were grown using a floating zone furnace [19]. BSCCO pieces with dimensions of approximately 3×3 mm were mounted to STM sample plates using conductive silver paste. After securing the STM sample plate to a scanning electron microscope (SEM) sample holder with double-sided carbon tape, the BSCCO surface was exfoliated using the Scotch tape method before being introduced into a Tescan Vega II SEM with base pressure of 2×10^{-5} mbar. Once under vacuum, hydrocarbons on the substrate surface were broken apart using the e-beam of the SEM as described previously [20]. Carbon clusters generated during this process were locally incorporated into locations between the layers of the substrate crystal. The extent of intercalation in the targeted region was distinguished by an increased height relative to the surrounding substrate controllable by the current, acceleration voltage, and exposure time of the beam.

Patterned intercalated regions with nanometer dimensions were achieved using DrawBeam software from Tescan. For this study, a square array of 1.5 μm spaced circular areas were intercalated. Each circle had a diameter of approximately 300 nm and height of roughly 4 nm as confirmed by ambient

*andrew.stollenwerk@uni.edu

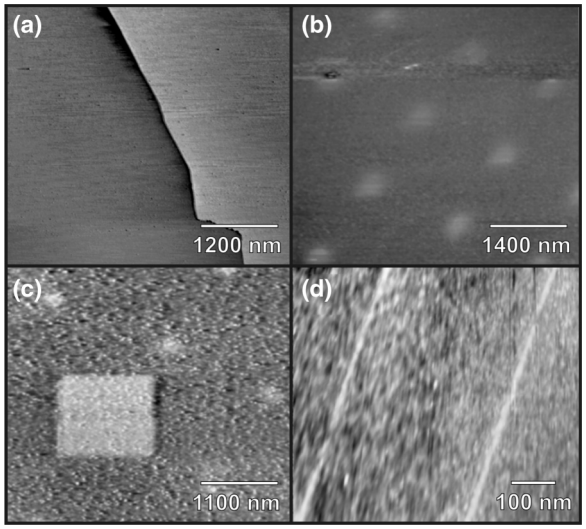

FIG. 1. STM images depicting the surface of (a) pure BSCCO and (b) an array of nanostructures resulting from local intercalation of carbon particles using an electron beam as described previously [20]. (c) STM image depicting a raised square structure resulting from a 1.2×1.2 μm scan at $V_{tip} = 1.6$ V and $I_{tip} = 4.4$ nA. (d) Linear features created from individual line scans at $V_{tip} = 1.0$ V and $I_{tip} = 1.0$ nA.

measurements using an Agilent 5500 AFM in noncontact mode. After this, samples were removed from the SEM sample holder and inserted into a variable-temperature (100–600 K) UHV STM system (Omicron) with a base pressure of 3×10^{-9} mbar to perform room temperature measurements. Tips were electrochemically etched from 0.15 mm W wire using a 5 M KOH solution and cleaned by scanning a sacrificial substrate until stable images and spectroscopy could be reliably reproduced. Resulting STM data were analyzed using the WSxM software [21].

III. RESULTS AND DISCUSSION

The surface of unaltered BSCCO samples were atomically flat with a low step density as seen in Fig. 1(a). Images of the sample surface after patterned intercalation such as Fig. 1(b) exhibit an array of circular structures with approximate diameter of 300 nm and average height of 3.39 ± 1.26 nm, consistent with the intended pattern. The surface of the circular structures and the surrounding substrate tend to have subnanometer roughness and are nearly as smooth as the surface prior to intercalation. Initially, to investigate surface quality above the intercalated regions in more detail, a 1.2×1.2 μm scan was taken centered on a single circular structure. Surprisingly, the image generated from this scan (not shown) is flat and featureless. The absence of the expected circular feature originally led to the belief that incorrect coordinates had been entered into the software. However, a subsequent image of the intended scan area shows the circular feature was replaced by the roughly 3.4 nm high square plateau seen in Fig. 1(c). The square structure shares the same lateral dimensions as the 1.2×1.2 μm scan suggesting it was formed during the preceding scan. This was later confirmed by examining the dimensions of similar raised structures formed using a variety of scan sizes ranging from 250×250 nm to 1.5×1.5 μm. The minimum feature size was determined to be on the order of 10 nm by examining single line scans such as those in Fig. 1(d). The width of linear structures formed in this manner could be as large as 100 nm and seemed to be mostly correlated with tip quality rather than any adjustable tunneling parameter. It is important to note that no raised features could be produced on either pure BSCCO or TiS_2 with a similar intercalated pattern.

During these experiments it was discovered that the larger scans used to characterize the raised structures had to be completed in a timely manner to minimize further modification of the surface. A scan with a 500×500 pixel resolution completed in 3.5 minutes over an area of 5×5 μm resulted in no noticeable changes in the surface for up to 4–7 consecutive scans. It was also discovered that a minimum distance of 10 μm is necessary between structures so that new structures are not formed at the expense of previous structures. To maintain consistency in subsequent experiments, all raised structures had dimensions of 550×550 nm and were formed using 500×500 dwell pixels acquired over a period of 3.5 minutes, unless otherwise noted. Resulting structures were afterwards characterized using a concentric 5×5 μm scan also composed of 500×500 pixels acquired over a period of 3.5 minutes and taken at a tip bias of 1.0 V and constant current of 1.0 nA.

Difficulties were common when attempting to acquire tunneling spectra on the original circular structures formed in the SEM. Rapid spikes in current or complete loss of signal were often observed and likely due to sudden changes in the sample surface. Nevertheless, a moderate quantity of stable spectra were collected with a representative spectrum displayed in Fig. 2. The inset in Fig. 2 depicts a histogram of the surface energy band gap extracted from the derivative of individual spectrum in a manner similar to that employed previously [22,23]. The modal value of the band gap is approximately 1.8 eV, consistent with optical absorption and photoluminescence results [20]. When compared to the metallic spectra of pure BSCCO in Fig. 2 it is clear that the addition of carbon intercalates locally modifies the electronic

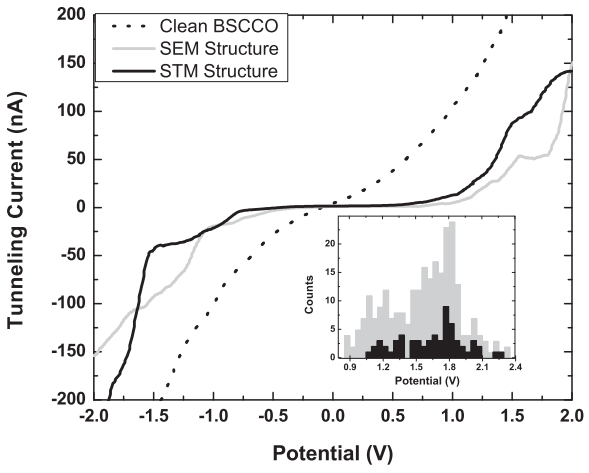

FIG. 2. Comparison of typical tunneling spectra obtained from unaltered BSCCO to that from nanostructures formed in the SEM and STM. Inset: Histogram of the surface energy band gap of the SEM and STM structures.

properties of the substrate surface. A representative spectrum obtained from a square structure formed in the STM is shown in Fig. 2. Although stability issues resulted in relatively fewer data points, the STM structures also exhibited a similar band gap distribution as seen in the inset of Fig. 2 overlaying the SEM structure data. The similarity of the spectra and the inability to form the raised structures on pure BSCCO suggest that the features formed in the STM are composed of the original carbon intercalates.

We observe a decrease in growth rate of the square structures for both consecutive scans and increased scan times. For example, when using a 1 V tip bias and 1 nA tunneling current, a 5 minute scan results in an 80% increase in height compared to a 1 minute scan. In contrast, when a 5 minute scan is increased to a 15 minute scan the height increases by only 20% instead of the 50% expected for linear growth. This behavior is consistent with dwindling quantities of carbon particles yet we do not detect a reduction in height of the surrounding circular structures outside noise levels. This was found to be the case even after creating a 550×550 nm structure with a height of 28 nm directly adjacent to an intercalated area. A noticeable reduction in growth rate without significant decreases in the original structures would appear to be in conflict with our previous supposition.

It is possible these inconsistencies can be resolved by examining the mechanism responsible for moving the particles the most obvious being the electric field generated by the tip. At first glance this is contradictory with the conductive nature of BSCCO which should screen the electric field within an angstrom of the surface, effectively inhibiting interaction with any subsurface carbon. However, there is evidence that the outermost BiO layer is semiconducting [24–27]. To better understand how the electric field interacts with the carbon particles, structures were created by scanning at different potentials. Cross-section line profiles from three of these structures and the corresponding images are shown in Fig. 3(a) for features formed at -0.5 V, -1.0 V, and -3.0 V. Initially, an increase in potential results in the movement of more material as would be expected if the electric field were playing a role in this process; however, the reduction in height at the higher potential is unexpected in this context. This relationship becomes more clear in the plot of height vs voltage displayed in Fig. 3(b) which shows the height peaks at roughly -1.0 V before declining, a pattern also present in the positive bias data with the peak occurring at about 1.7 V. This range coincides with the band gap of the uppermost BiO layer, experimentally determined to be 2.5–3 eV [25]. At lower voltages there are no available states in the top BiO layer or the insulating SrO layer directly beneath, so that tunneling occurs primarily through the CuO_2 layer about 4.5 Å below the surface. As states in the BiO layer open up at higher biases the feedback loop retracts the tip by up to 3–4 Å, reducing the strength of the electric field by roughly doubling the separation between the tip and sample [25] and accounting for the sudden drop in material moved. In this case, a substrate with metallic layers would prevent manipulation of any subsurface carbon as is observed in the case with TiS_2. In addition, the limited quantity of near surface carbon would likely be depleted quickly without significantly reducing the size of the circular structures given that the majority of intercalates deeper in the sample remain intact.

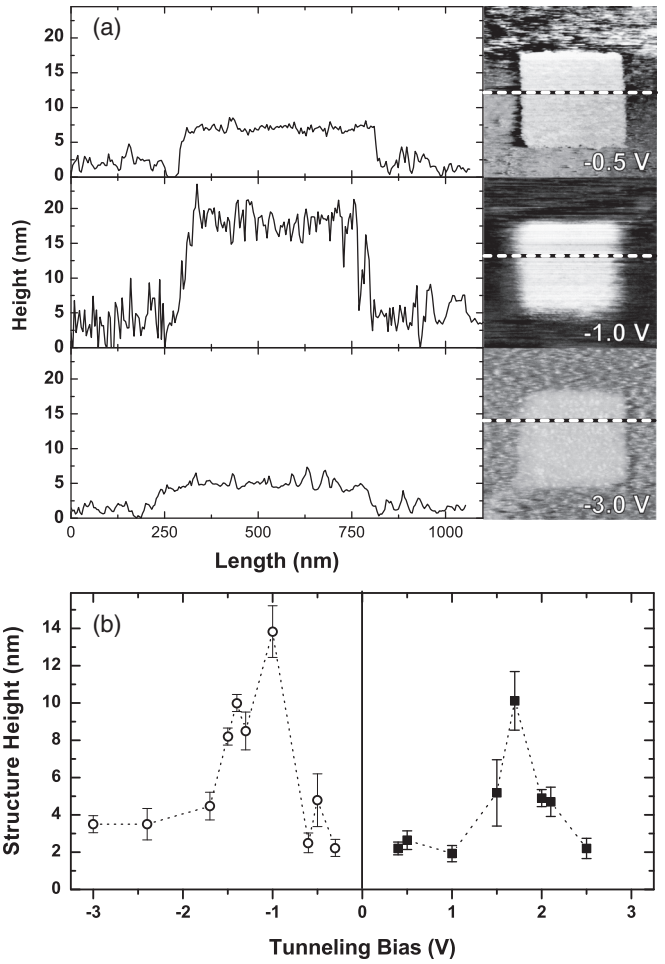

FIG. 3. (a) Line profiles and corresponding characterization images of different structures acquired using tunneling parameters of $V_{tip} = 1$ V and $I_{tip} = 1$ nA. Structures depicted here were formed by first scanning a 550×550 nm area at a tip bias of -0.5, -1.0, and -3.0 V and a constant tunneling current of 1.0 nA prior to the characterization scan. (b) Relative heights of structures formed at various tip biases.

Perhaps most interesting is whether the carbon remains subsurface when transported across the sample. In layered materials such as BSCCO, movement of intercalates perpendicular to the basal plane is generally more difficult than intraplane movement due to the strong lateral bonds forming the molecular layers. This would suggest that subsurface transport between layers is favorable, but damage to the crystal lattice ensuing from the intercalation process could facilitate extraction of subsurface carbon. A number of high-resolution scans were taken using a variety of parameters to better understand where the carbon particles reside after they are transported to the scan area. Unfortunately, tunneling conditions during these scans tended to be unstable due to the dynamic topography of the surface. The image depicted in Fig. 4(a) was obtained at a tip bias of 0.6 V and tunneling current of 1.0 nA and is representative of the limited number of stable scans acquired during the process of creating a 550×550 nm square structure. The clusters in this image are presumed to be carbon particles relocated to the scan area and have an average

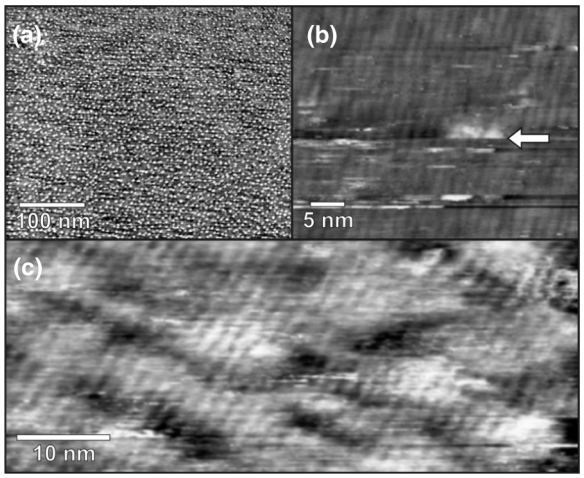

FIG. 4. (a) STM image acquired while scanning at $V_{tip} = 0.6$ V and $I_{tip} = 1.0$ nA. (b) High-resolution image taken at $V_{tip} = 0.6$ V and $I_{tip} = 4.4$ nA showing the appearance of carbon clusters midscan exemplified by the arrow. (c) High-resolution image taken at $V_{tip} = 0.5$ V and $I_{tip} = 1.8$ nA with protrusions in the surface up to 1.2 nm.

height of 0.9 ± 0.3 nm. The average diameter is approximately 2.4 ± 0.7 nm including tip convolution effects.

A limited number of high-resolution images were acquired such as those seen in Figs. 4(b) and 4(c). These images were obtained from different locations in empty regions between circular structures. Both exhibit clusters similar to those in Fig. 4(a) but with greater detail. The image in Fig. 4(b) was taken at $V_{tip} = 0.6$ V and $I_{tip} = 4.4$ nA and exhibits corrugated features with dimensions consistent with the superstructure previously observed on BSCCO [27,28]. A sharp change in height parallel to the scan direction, such as that indicated by the arrow, is the result of a change in topography from one line scan to the next due to the appearance or disappearance of a cluster. The surface of the cluster indicated by the arrow appears to be irregular suggesting that it lies on the surface of the sample. It is therefore concluded that this and other such particles were either already on the surface prior to transport or were extracted from subsurface locations. The image depicted in Fig. 4(c) was taken at $V_{tip} = 0.5$ V and $I_{tip} = 1.8$ nA and appears to be have been acquired under more stable tunneling conditions than the image in Fig. 4(b). The protrusions from the surface in this image share the same corrugated features as the substrate and have relative heights that range from approximately 0.4–1.2 nm. The protrusions in this and other similar images must necessarily represent physical topographic increases as local density of state considerations alone would manifest as depressions. Because these results are not observed on pure BSCCO we conclude that the appearance of such protrusions ensues from the subsurface transport of intercalated carbon particles. Therefore, it seems that the raised structures formed while scanning the surface are composed of both surface and subsurface carbon particles.

IV. CONCLUSIONS

In conclusion, evidence has been presented indicating that the STM is able to manipulate subsurface carbon particles in BSCCO using the electric field generated by the tip. Using this carbon, structures with feature sizes down to approximately 10 nm can be created consisting of both surface and subsurface carbon particles. The semiconducting nature of these structures could possibly be exploited to form arrays of nanoscale Josephson junctions. Additionally, further research could demonstrate the applicability of this technique to other layered materials.

ACKNOWLEDGMENTS

This work was supported in part by the National Science Foundation, Grants No. DMR-1206530 and No. DMR-1410496. T.E.K. and R.H. acknowledge support from Iowa NASA EPSCoR under Grant No. NNX09AO66A. R.H. also acknowledges support from the American Chemical Society Petroleum Research Fund, Grant No. 53401-UNI10. A pre-tenure summer fellowship for A.J.S. and R.H. was made available through the University of Northern Iowa. Work at Brookhaven is supported by the Office of Basic Energy Sciences, Division of Materials Sciences and Engineering, U.S. Department of Energy, under Contract No. DE-AC02-98CH10886. The authors thank B. Adams for useful discussions.

[1] S. G. Corcoran, R. J. Colton, E. T. Lilleodden, and W. W. Gerberich, Phys. Rev. B **55**, R16057 (1997).
[2] U. Landman, W. D. Luedtke, N. A. Burnham, and R. J. Colton, Science **248**, 454 (1990).
[3] B. Parkinson, J. Am. Chem. Soc. **112**, 7498 (1990).
[4] J. L. Huang, Y.-E. Sung, and C. M. Lieber, Appl. Phys. Lett. **61**, 1528 (1992).
[5] D. M. Eigler and E. K. Schweizer, Nature (London) **344**, 524 (1990).
[6] J. A. Stroscio and D. M. Eigler, Science **254**, 1319 (1991).
[7] J. A. Stroscio, F. Tavazza, J. N. Crain, R. J. Celotta, and A. M. Chaka, Science **313**, 948 (2006).
[8] I. Lyo and P. Avouris, Science **253**, 173 (1991).
[9] S. W. Hla, K. F. Braun, and K. H. Rieder, Phys. Rev. B **67**, 201402 (2003).
[10] J. J. Boland, Science **262**, 1703 (1993).
[11] D. A. Olyanich, V. G. Kotlyar, T. V. Utas, A. V. Zotov, and A. A. Saranin, Nanotechnol. **24**, 055302 (2013).
[12] S. Fölsch, J. Martínez-Blanco, J. Yang, K. Kanisawa, and S. C. Erwin, Nat. Nanotechnol. **9**, 505 (2014).
[13] E. C. H. Sykes, L. C. Fernández-Torres, S. U. Nanayakkara, B. A. Mantooth, R. M. Nevin, and P. S. Weiss, Proc. Natl. Acad. Sci. USA **102**, 17907 (2005).
[14] H. Zheng, A. Weismann, and R. Berndt, Phys. Rev. Lett. **110**, 226101 (2013).
[15] L. B. Ioffe, V. B. Geshkenbein, M. V. Feigel'Man, A. L. Fauchere, and G. Blatter, Nature (London) **398**, 679 (1999).
[16] Y. Kubo, A. O. Sboychakov, F. Nori, Y. Takahide, S. Ueda, I. Tanaka, A. T. M. N. Islam, and Y. Takano, Phys. Rev. B **86**, 144532 (2012).

[17] R. Kleiner and P. Müller, Phys. Rev. B **49**, 1327 (1994).
[18] M. Götte, T. Paananen, G. Reiss, and T. Dahm, Phys. Rev. Appl. **2**, 054010 (2014).
[19] G. Gu, K. Takamuku, N. Koshizuka, and S. Tanaka, J. Cryst. Growth **130**, 325 (1993).
[20] T. E. Kidd, A. O'Shea, B. Beck, R. He, C. Delaney, P. M. Shand, L. H. Strauss, A. J. Stollenwerk, N. Hurley, K. Spurgeon, and G. Gu, Langmuir **30**, 5939 (2014).
[21] I. Horcas, R. Fernández, J. M. Gómez-Rodríguez, J. Colchero, J. Gómez-Herrero, and A. M. Baro, Rev. Sci. Instrum. **78**, 013705 (2007).
[22] Y. Lin, R. Lin, W. Wang, and X. Xiao, Appl. Surf. Sci. **143**, 169 (1999).
[23] K. Hata, Y. Shibata, and H. Shigekawa, Phys. Rev. B **64**, 235310 (2001).
[24] Y. Gao, P. Lee, P. Coppens, M. A. Subramania, and A. W. Sleight, Science **241**, 954 (1988).
[25] C. K. Shih, R. M. Feenstra, and G. V. Chandrashekhar, Phys. Rev. B **43**, 7913 (1991).
[26] C. K. Shih, R. M. Feenstra, J. R. Kirtley, and G. V. Chandrashekhar, Phys. Rev. B **40**, 2682 (1989).
[27] M. D. Kirk, J. Nogami, A. A. Baski, D. B. Mitzi, A. Kapitulnik, T. H. Geballe, and C. F. Quate, Science **242**, 1673 (1988).
[28] S. Sugita, T. Watanabe, and A. Matsuda, Phys. Rev. B **62**, 8715 (2000).